TECHNICAL ARTICLE—PEER-REVIEWED

Fatigue Behavior of Welded API 5L X70 Steel Used in Pipelines

Şermin Özlem Turhan · Ali Motameni · Rıza Gürbüz

Abstract In this study, fatigue failure behavior of welded X70 pipeline steel was investigated by rotating bar bending fatigue tests performed at room temperature. *S–N* curves of base metal, weld and heat-affected zone (HAZ) were plotted. Tension tests, hardness measurements and Charpy V-notched impact tests were carried out for mechanical characterization. Samples were examined with optical microscope and scanning electron microscope (SEM) microstructurally. Fracture surfaces were examined with SEM. In addition to fractographic analysis, striation counting method was used to estimate the crack growth rate of base metal, weld and HAZ. Stress intensity factor (ΔK) ranges were also calculated. Tensile properties and hardness values of base metal and weld were found to be almost the same. Charpy impact test results show that base material has approximately twice impact energy than weld and HAZ at room temperature. However, Charpy impact energies of HAZ and weld decreased noticeably at − 30 °C, while very slight decrease was observed for base metal. The comparison of high-cycle fatigue and crack growth behaviors shows that base metal has better fatigue behavior of all from the point of crack initiation and propagation. Moreover, our findings also support the idea that striation counting can be used as a fractographic approach to estimate the crack growth behavior of materials.

Ş. Ö. Turhan (✉) · R. Gürbüz
Metallurgical and Materials Engineering Department, Middle East Technical University, 06800 Ankara, Turkey
e-mail: sermin.turhan@metu.edu.tr

A. Motameni
Faculty of Engineering, Middle East Technical University, 06800 Ankara, Turkey

Keywords Pipeline steels · Fatigue · *S–N* curve · X70 steel · Striation spacing

Introduction

In recent years, with the increase in the production and consumption of crude oil and natural gas worldwide, the transport of materials used in energy and petrol sectors is of strategic importance [1, 2]. This has made production, installation and operation of large diameter pipes used at very long distances and under high-pressure conditions important in terms of economy and safety [3, 4]. The 70% of energy transportation worldwide are carried out by pipelines [2]. There are also other ways of transportation on land such as trucks and trains for crude oil. However, when they are compared with transportation by pipelines, it is seen that transport through the pipelines is more economical and safer [5].The transportation of iron ore to long distances with pipelines has brought a solution also for mining sector [2]. In addition to these materials, pipelines also transport hydrogen and dangerous liquids such as LPG, gasoline and refined petroleum products [1, 6].

When considering the sectors where the pipes are used, the pipes could work at high pressures and have necessarily large diameters in order to decrease the cost and increase the efficiency of transport [2, 4]. Pipelines used in natural gas and oil transportation may be exposed to the plastic deformation caused by external forces such as landslides [7]. Another external factor is the fluctuation in pressure due to corrosive environment. In this case, fatigue behavior gains importance in design [8]. The damages occurred in pipelines can cause many serious consequences from air, lake and river pollution to human injuries [1]. For these

reasons, the pipeline material and the connected systems require good mechanical properties with having excellent welding and corrosion resistance that can withstand external impacts and negative effects [7, 8].

The main material of the pipes used in oil or natural gas transport is 97% the hot-rolled coils. Most of the line pipes used today are manufactured according to API 5L or EN ISO 3183 (DIN EN 10208-2) Standards [1]. For a very long time, API 5L X42, X52, X60, X65 steels have been used for these pipes, but for later high strength requirements, X70 and X80 steels are developed and now preferred worldwide. [1, 7]. X70 pipeline steel is good in strength and toughness in addition to having great weldability and corrosion resistance [9]. X70 grade has been also widely used in the offshore industry for many years due to having great toughness and weldability properties. However, in terms of design and requirements, pipelines generally differ from offshore structures [10].

The durability of pipelines subjected to high pressure depends not only on the wall thickness of the pipe and the material structure but also on the quality of weld joints without cracks [11, 12]. Helical or longitudinal welded pipes produced by submerged arc welding (SAW) are mostly preferred in gas and oil transmission lines [7, 13]. Helical welded pipes are produced from hot-rolled coils, while longitudinal welded pipes are produced from plate or coil [1]. SAW is used because of the easy control of the variables in the process, high quality, smooth welding, protection of the welding arc zone from the atmosphere and ease of automation process in welding process. The welding parameters used in submerged arc welding play an important role in the quality of the weld joint [12].

There have been many studies conducted on the mechanical properties of welded pipelines. However, studies on fatigue behavior have been one sided, focusing either on crack initiation or propagation. Searching fatigue properties in pipeline steels is a serious concern as sudden failures could occur under cycling loadings created by pressure fluctuations in a corrosive environment during transportation [2, 8, 14]. This study has been conducted in order to have an integrated approach on fatigue behavior of welded pipelines. Within this scope, welded API 5L-X70M-PSL2 pipeline steel was subjected to the investigation.

For mechanical characterization tension tests, hardness measurements and Charpy impact tests were carried out. Samples were examined with optical microscope and scanning electron microscope (SEM) microstructurally. Rotating bending fatigue tests of base material, weld and heat-affected zone (HAZ) were performed at room temperature according to the international ISO 1143:2010 Standard and S–N curves were plotted. Fracture surfaces were examined with SEM. Since pipeline steels eventually

fracture due to crack propagation through the wall thickness of the pipe, it is important to study crack growth rate in fatigue failure [15]. In this context, striation spacings were measured with fractographic analysis and crack growth rates (da/dN) were estimated for base metal, weld and HAZ. Stress intensity factor (ΔK) ranges were also calculated with striation counting method and da/dN versus ΔK curves were plotted in log scale for all test groups.

Experimental Procedure

Material and Production Process

In this study, API 5L-X70M-PSL2 pipeline steel, which is a kind of HSLA, was used for investigation. The specimens were prepared from helical welded pipes produced from hot-rolled X70 coils with SAW method. S2 Mo welding wire was used as an electrode and P223 welding powder was used as a protective powder during the joining processes. Welding parameters and geometry are given in Table 1 and Fig. 1, respectively. Chemical composition of the API 5L X70 steel and weld material is given in Tables 2 and 3. X70 steel meets the requirements of chemical composition in API Specifications 5L.

Microstructural Analysis

Two different specimens were prepared in transverse and longitudinal directions for microstructural analysis with optical microscope. Specimens were etched with 2% Nital. The specimen prepared in transverse direction comprises regions of weld and HAZ (Fig. 2). HAZ has three different microstructures due to different cooling rates during welding. So all these regions which were called as HAZ1 (coarse-grained region), HAZ2 (grain-refined region) and HAZ3 (inter-critical region) were subjected to investigation.

Mechanical Analysis

Tensile properties of both base metal and weld zone were examined with 100 kN Instron Universal Tension/

Table 1 Welding parameters

	Current (A)		Voltage (V)		Welding speed (cm/min)
	DC	AC	DC	AC	
Inside	1000 ± 100	675 ± 67.5	29 ± 2	32 ± 2	130 ± 13
Outside	1100 ± 110	650 ± 65	30 ± 2	34 ± 2	130 ± 13

Compression Testing Machine (the load cell of the machine is certified) according to ISO 6892-1:2016 Standard.

Vickers hardness test method was used to measure the hardness values of base metal, HAZ and weld metal according to ISO 6507-1:2018 Standard. Hardness values were taken from three different lines in transverse direction.

Charpy impact specimens with a V-notch were prepared from base metal, HAZ and weld metal according to ISO 148-1:2016 Standard in transverse direction. For the analysis of HAZ, one type of specimens was prepared from 1 mm right of the fusion line (FL1) and the others were prepared 2 mm right of the fusion line (FL2). In each type of specimens, three samples were prepared with a size of 10 mm × 10 mm × 55 mm and a V-notch of 2 mm deep. Charpy V-notch impact tests were carried out using certified Tinius Olsen Pendulum Impact Tester (406 J).

Rotating Bending Fatigue Test

Rotating bending fatigue tests were conducted according to the ISO 1143:2010 Standard at room temperature and a nominal frequency of 30 Hz. The rotating bending testing machine with a servo motor having capacity of maximum 3000 rev/min was used for the tests. Identical specimens in hourglass type were prepared in transverse direction with base metal, HAZ and weld metal are in the middle of the specimen. In the welded specimen, to see if the weld has coincided with the center of the specimen, it was etched with 10% Nital. All test groups were subjected to single point loading with a stress ratio of − 1 ($R = − 1$). The geometry of hourglass-type specimen, the moment (M) diagram and the stress (σ) distribution along the specimen is shown in Fig. 3. Stress reaches maximum value at the center of the specimen where the cross section is smallest, while moment increases along the specimen. The distribution of stress at the cross section is shown in Fig. 4. Stress value corresponding to a given load on a rotating beam test machine was calculated by the below formula derived according to Theory of Simple Bending and the formula was confirmed by using strain gage method.
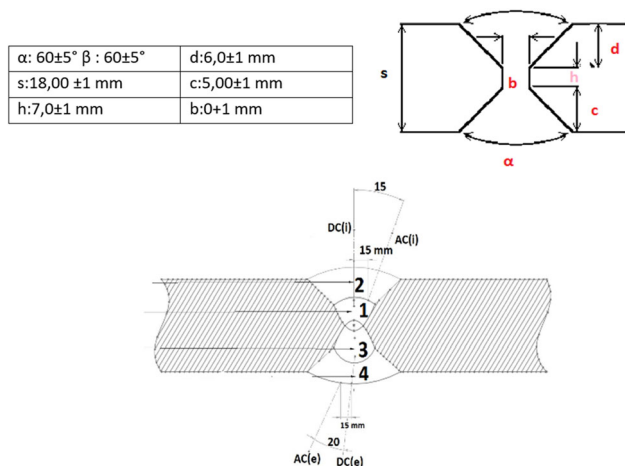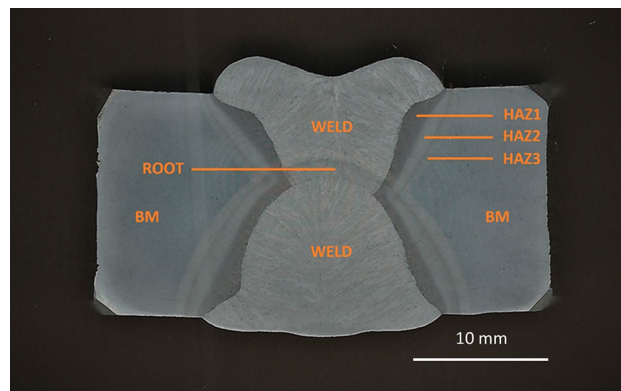

Fig. 1 Welding groove geometry

Fig. 2 The specimen prepared for microstructure analysis in transverse direction

Table 2 Chemical composition of API 5L X70 steel

	C	Si	Cu	Fe	Mn	Mo	P	S	Ni	Cr	V	Nb	Al
Wt.%	0.06	0.39	0.04	97.43	1.58	0.11	0.01	< 0.01	0.05	0.21	< 0.01	0.06	0.03

Table 3 Chemical composition of weld metal

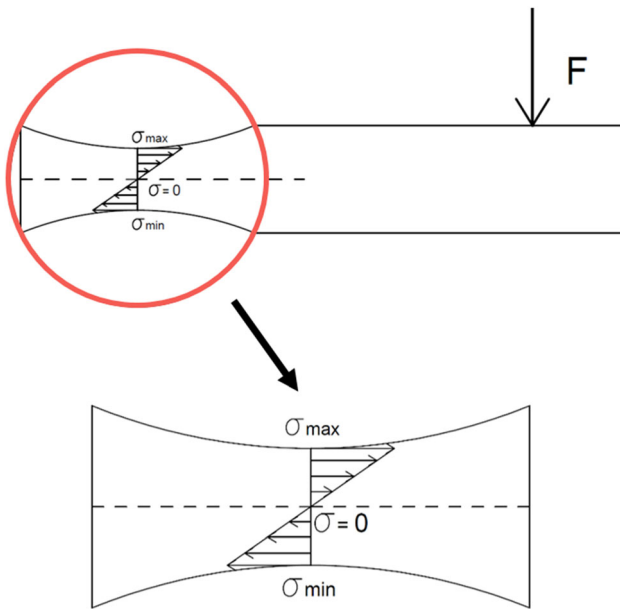|	C	Si	Cu	Fe	Mn	Mo	P	S	Ni	Cr	V	Nb	Al
Wt.%	0.06	0.39	0.07	97.43	1.48	0.24	0.01	< 0.01	0.05	0.17	< 0.01	0.04	0.02

Fig. 3 Geometry of hourglass-type specimen and the corresponding moment (M) and stress (σ) diagrams as a function of the distance (x)
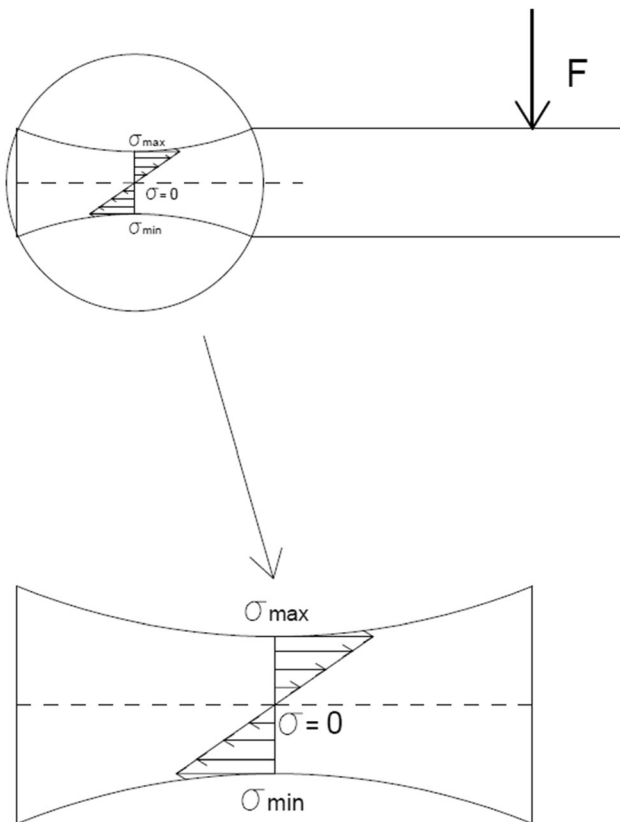

Fig. 4 Stress distribution along the smallest cross section of the specimen
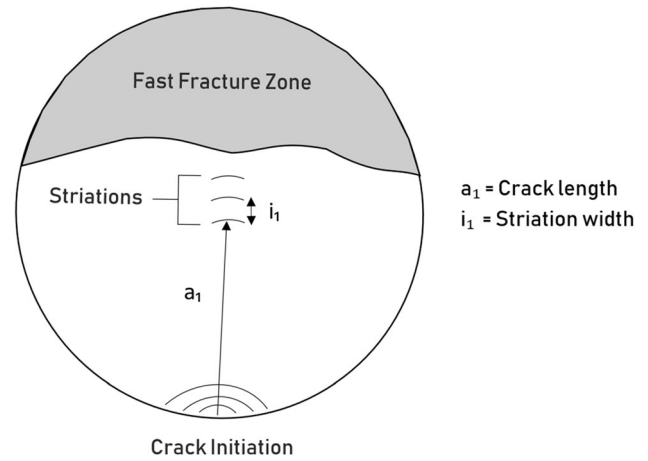

Fig. 5 Striation counting method

$$\sigma = \frac{32FL}{\pi d^3}.$$

Fractographic Analysis

Fracture surfaces of different type of specimens subjected to rotating bending fatigue test were examined with visual inspection first and then detail analysis was performed with SEM. The fracture surfaces were analyzed from the point of morphology and fatigue failure features. In addition, striation counting method was used, in order to examine the crack growth behavior of each test groups. With this method, striation width was measured at a certain point and then the distance between that point and crack initiation point was measured as shown in Fig. 5. Stress intensity factor for a surface crack in a solid cylinder is calculated by below formulas given in Table 4 [16]. Then, crack growth rate (da/dN) versus stress intensity factor (ΔK) in log scale was plotted for base metal, weld and HAZ.

Results and Discussion

Microstructural Analysis

The microstructure of base material was determined to be uniform and fine acicular ferrite in transversal cut and rolling direction is clearly seen in longitudinal cut in Fig. 6. When the optical micrographs taken from transversal cut in

1558

J Fail. Anal. and Preven. (2020) 20:1554–1567

Table 4 Stress intensity factor solution for solid cylinder [16]
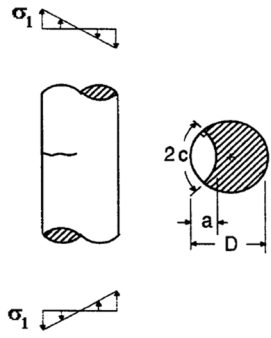
Stress Intensity Factor	$K_1 = F_1 \sigma_1 \sqrt{\pi a}$
	$F_1 = G \left[0.923 + 0.199 \, Y^4 \right]$ $G = 0.92 \left(\dfrac{2}{\pi} \right) sec \, \beta \left[\dfrac{(tan \, \beta)}{\beta} \right]^{\frac{1}{2}}$ $Y = 1 - sin \, \beta$ $\beta = \left(\dfrac{\pi}{2} \right) \left(\dfrac{a}{D} \right)$

Fig. 6 Optical micrographs of base metal region of X70 steel; (**a**) transversal cut; AF (acicular ferrite) and (**b**) longitudinal cut at ×1000 magnification
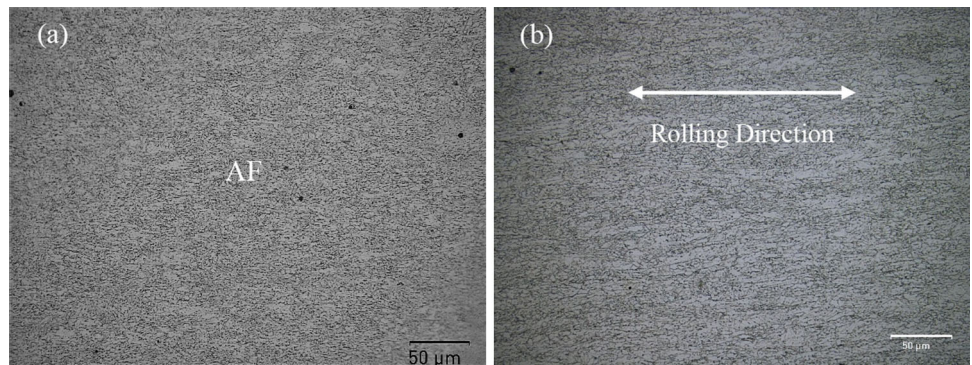
Fig. 7 Optical micrographs of weld region and HAZ subregions; (**a**) weld metal, (**b**) HAZ1, (**c**) HAZ2 and (**d**) HAZ3 at ×1000 magnification
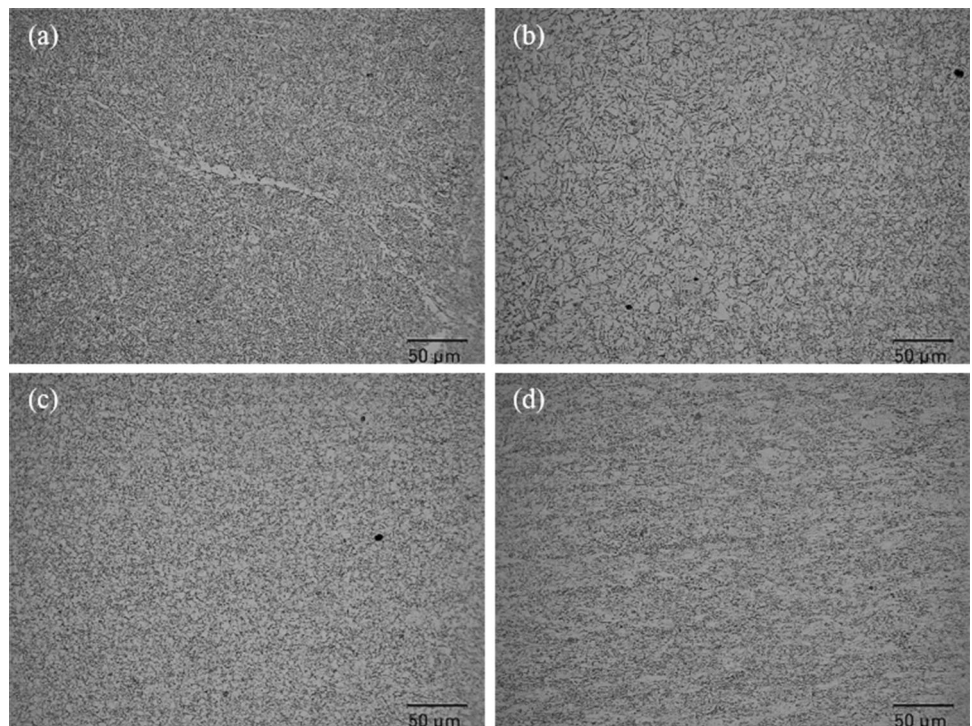
Table 5 Tensile test results of specimens from base metal region of X70 steel

Specimen no.	Maximum tensile stress (MPa)	Tensile stress at yield (offset 0.2%) (MPa)	Axial strain at break (%)
X70 steel			
1 (Transverse)	727	657	18
2 (Transverse)	712	637	21
Average	720	647	20
Weld			
1 (Longitudinal)	711	656	22
2 (Transverse)	714	638	14
Average	713	647	18

Fig. 8 Hardness profiles of lower line, midline and upper line along the base metal, HAZ and weld
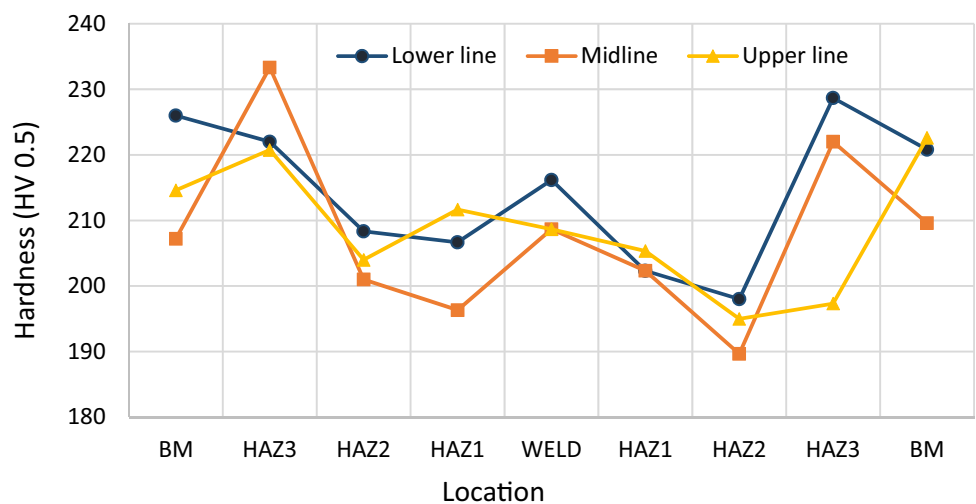
Fig. 7 were examined, it is clearly seen that grain size is the largest at the closest region to the weld section (HAZ1). Due to the growing grains in this region, larger, complex and amorph grain structure was observed. However, grain size of HAZ2 is very small compared to the HAZ1 and the grains distributed homogeneously with equiaxed grain structures. The microstructure of HAZ3 seems more like the base metal's microstructure.

Mechanical Analysis

In Table 5, the basic mechanical properties of the X70 steel and welded zone obtained from tensile tests are given. Tensile requirements for Grade X70 PSL 2 were provided. The results of the tensile tests showed that the mechanical properties of weld metal are almost the same as the base metal. The examination of the fracture surfaces of the specimens shows that fracture is ductile for both base metal and weld. The fracture was observed in the weld section of specimen prepared in transverse direction and this result is proportional to the higher tensile strength of the base material than the weld metal.

In Fig. 8, the average hardness values are shown for the lines separately, while Fig. 9 shows the hardness profiles for midline and the average of lower and upper lines. The reason of taking average of upper and lower lines is the similarity between cooling rates and expected hardness profiles. In Fig. 8, it is seen that HAZ3 has the highest hardness value for midline and lower line, whereas HAZ2 has the lowest hardness value. For the upper line, the highest hardness value was observed in base metal, whereas HAZ2 has the lowest hardness value again. It is thought that the phases occur due to heating and cooling in the weld metal, residual stresses in the weld zone and the additional welding wire and powder combination cause higher hardness values in the weld metal [7]. However, hardness values of the base metal are a lit bit higher than the weld metal and they both have higher hardness values

1560

J Fail. Anal. and Preven. (2020) 20:1554–1567

Fig. 9 Hardness profiles of midline and upper/lower line avg. along the base metal, HAZ and weld
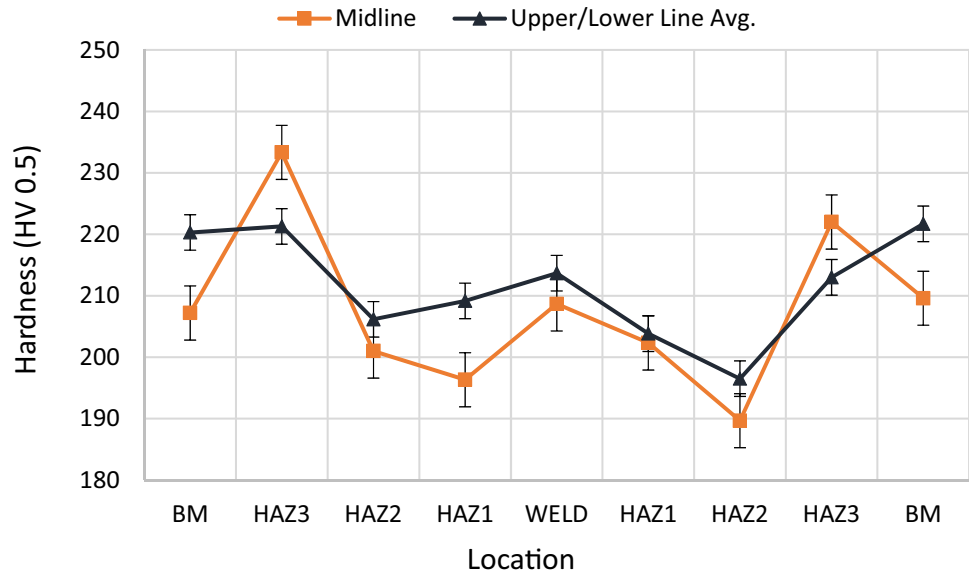

Table 6 Charpy impact test results at 25 and − 30 °C or BM, fusion line 1, fusion line 2 and weld

Sample	No.	Impact energy (J) for 25 °C	Fracture behavior at 25 °C	Impact energy (J) for − 30 °C	Fracture behavior at − 30 °C
Base metal	1	335	100% ductile	282	100% ductile
	2	312	100% ductile	315	100% ductile
	3	335	100% ductile	308	100% ductile
	X_m	327 ± 13		302 ± 17	
Fusion line 1	1	163	82% ductile	124	67% brittle
	2	186	92% ductile	63	100% brittle
	3	150	86% ductile	80	100% brittle
	X_m	166 ± 18		89 ± 31	
Fusion line 2	1	210	100% ductile	60	100% brittle
	2	207	100% ductile	59	100% brittle
	3	121	52% ductile	77	89% brittle
	X_m	179 ± 51		65 ± 10	
Weld	1	143	92% ductile	56	100% brittle
	2	168	100% ductile	60	100% brittle
	3	143	100% ductile	76	49% brittle
	X_m	151 ± 14		64 ± 11	

than HAZ2 and HAZ1. When Fig. 9 was examined, it is clearly seen that the average hardness values are higher than the midline's hardness values expect for HAZ3.

Table 6 shows the Charpy impact test results at 25 and − 30 °C for base metal, fusion line 1 (FL1) and fusion line 2 (FL2) and weld metal. It is seen that Charpy impact energies of heat-affected zone (FL1 and FL2) and weld metal decreased noticeably when the test temperature decreased from 25 to − 30 °C. However, very slight

decrease was observed for the base metal as the temperature decreased. Base metal has the highest toughness of all regions for both test temperatures. The reason for base metal having better toughness is fine microstructure obtained due to thermo-mechanical control process (TMCP). The reason for weld having the worst toughness could be the columnar coarse grains and inhomogeneous microstructure in weld region. The test results at 25 °C shows that, the lowest impact energies observed in weld
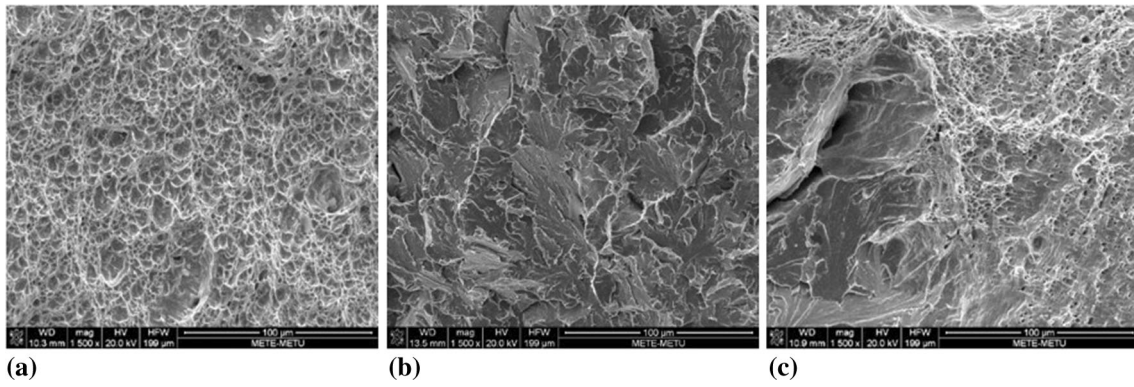
J Fail. Anal. and Preven. (2020) 20:1554–1567

1561

Fig. 10 SEM images taken from FL2 tested at (**a**) 25 °C (No1), (**b**) − 30 °C and (**c**) 25 °C (No3)

Fig. 11 S–N plot for base metal

$$y = 860.67x^{-0.063}$$
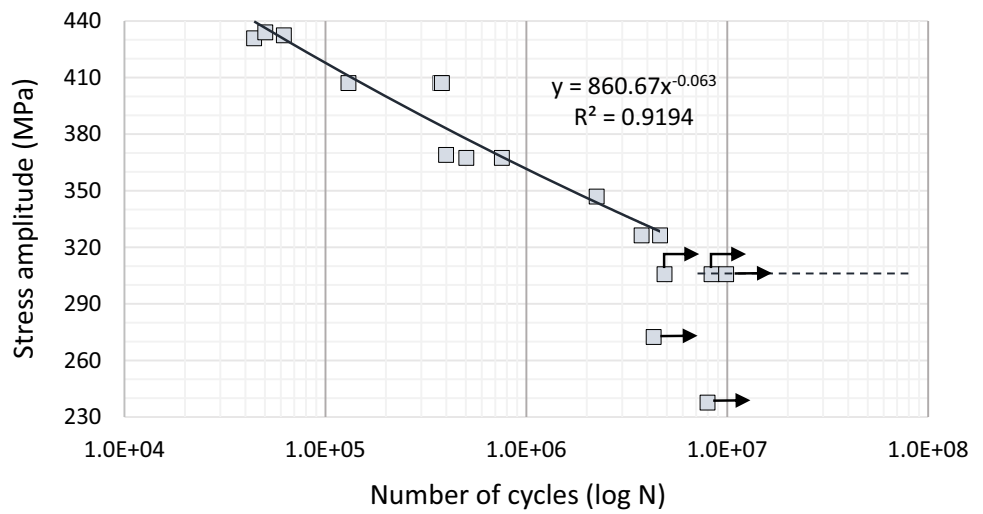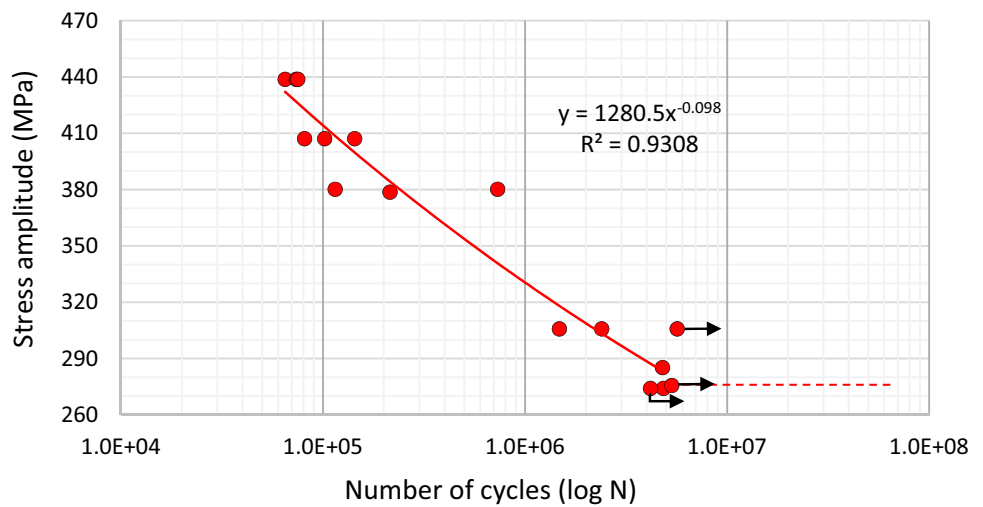$$R^2 = 0.9194$$

Fig. 12 S–N plot for weld metal

$$y = 1280.5x^{-0.098}$$
$$R^2 = 0.9308$$

metal, fusion line 1, fusion line 2 and base metal, respectively. For -30 °C, fusion line 2 and weld zone have almost the same impact energy, while fusion line 1 has higher impact energy than they have. According to the ASTM A370 Standard, the minimum impact energy that API 5L X70 steel should have is 60 J at − 15 °C [7]. The test

1562

J Fail. Anal. and Preven. (2020) 20:1554–1567

Fig. 13 *S–N* plot for HAZ

$$y = 1377.4x^{-0.099}$$
$$R^2 = 0.9447$$
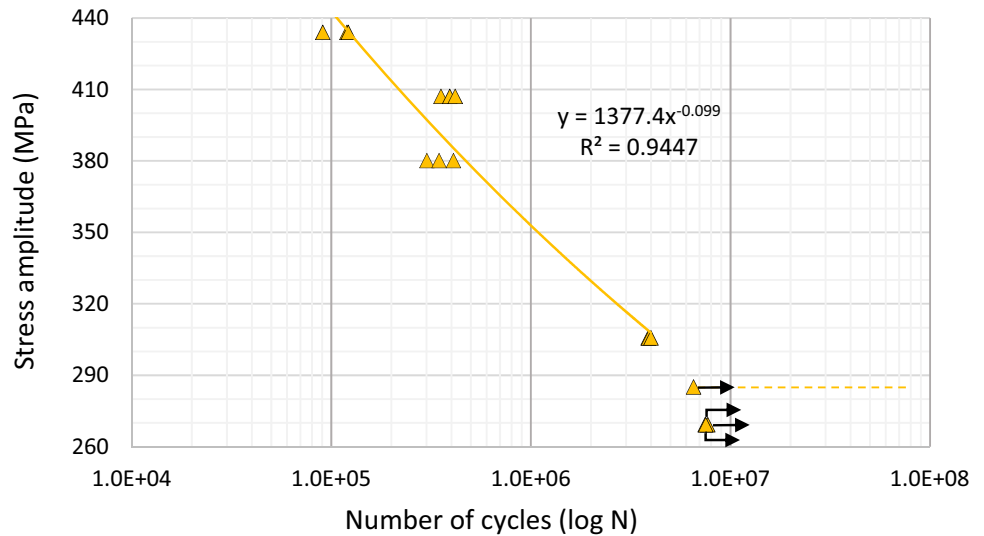
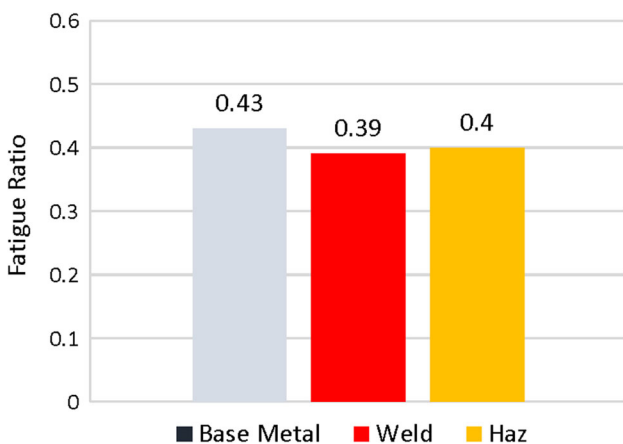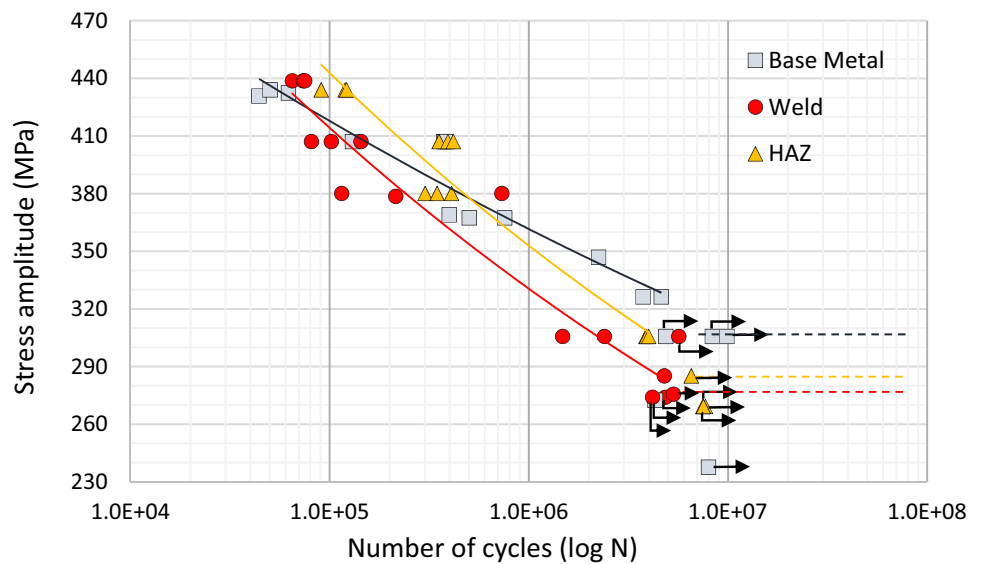**Fig. 14** *S–N* curves for base metal, weld and HAZ

Fig. 15 Fatigue ratios for base metal, weld and HAZ

results show that the weld metal and the HAZ region have higher impact energies than 60 J even at − 30 °C.

When the fracture surfaces were examined with SEM, dimples were observed for ductile type of fracture behavior, while cleavage planes were observed for brittle type of fracture behavior in Fig. 10a and b. For mix type of fracture behavior, both dimples and cleavage planes were observed as shown in Fig. 10c.

Rotating Bending Test Results

Rotating bending fatigue tests were conducted for X70 steel, weld and HAZ at similar stress levels. Stress (*S*) versus number of cycles (*N*) for failure plots is shown in Figs. 11, 12 and 13. The data for regression lines do not include the run-out stress values shown with arrows in *S–N*

J Fail. Anal. and Preven. (2020) 20:1554–1567

1563

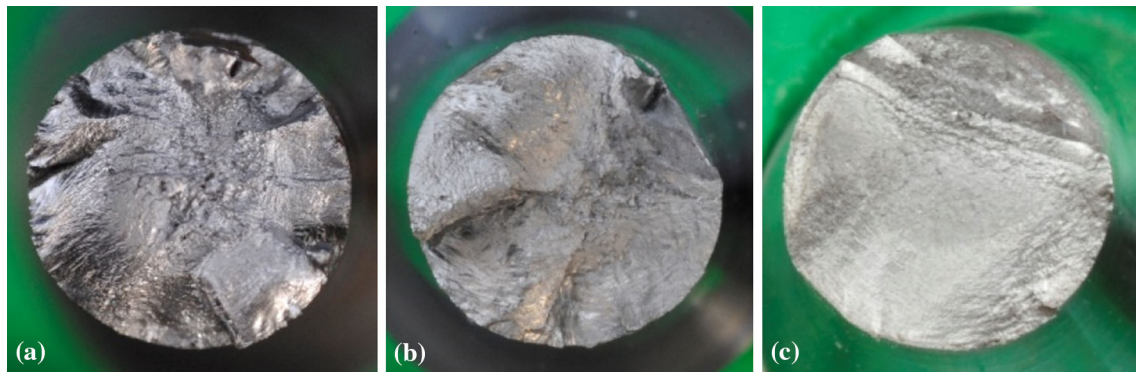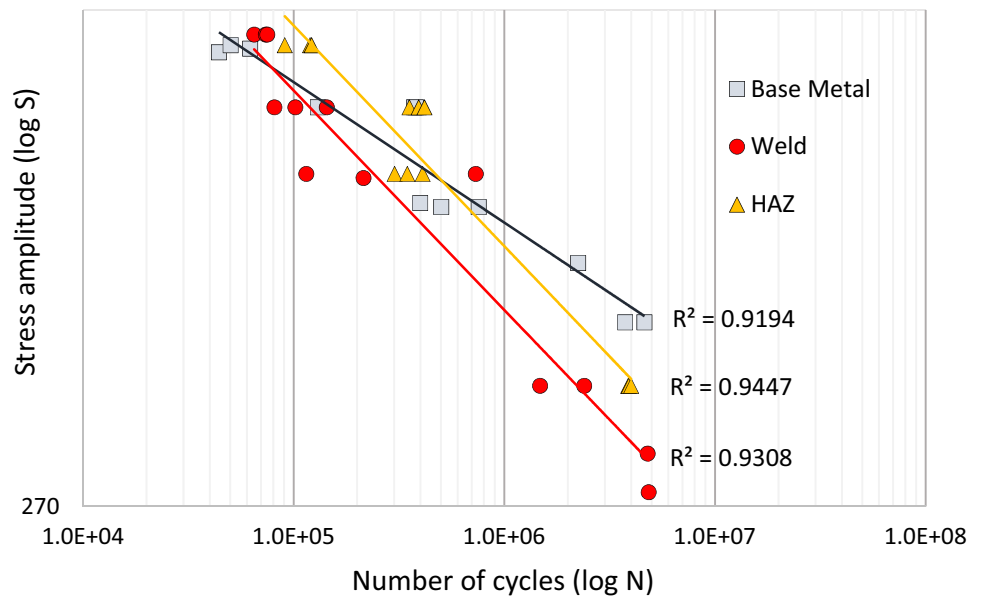**Fig. 16** Basquin slopes for base metal, weld and HAZ

Fig. 17 Macro-fracture surfaces of all test groups subjected to rotating bending fatigue test ($\sigma = 434$ MPa); (**a**) base metal, (**b**) weld and (**c**) HAZ

plots. Since coefficient of determination (R^2) value for base metal is 0.85 and higher than 0.9 for weld and HAZ, it is clear that regression lines for S–N plot represent the data points.

The fatigue test data for all test groups are shown in Fig. 14. It is obviously seen that the fatigue life of weld at any stress level is lower than base metal and HAZ. The endurance limit of weld is also lower than base metal and HAZ. When base metal and HAZ are compared, it is seen that at higher stress levels than approximately 380 MPa, HAZ has longer fatigue life. However, when the stress applied decreases below 380 MPa, the fatigue life of base metal is higher than HAZ's fatigue life (Fig. 14). The endurance limit of base metal is higher than HAZ's endurance limit. This result is also seen in Fig. 15 where fatigue ratios (σ_e/σ_{UTS}) of base metal, weld and HAZ are compared. The fatigue ratios of all three test groups were found to be within the range specified for steels [17, 18].

Basquin slopes were also calculated by plotting S–N curves on a log–log scale as shown in Fig. 16.

Fractographic Analysis

When the fracture surfaces were examined, at higher stress levels, multiple crack formation was observed for X70 steel and weld region, while it was not observed in HAZ at any stress level (Fig. 17). The ratchet markings, which are the indicators of multiple crack initiation and propagation, are shown at the fracture surface of base metal failed at high stress level (Fig. 18a). Dimples were observed indicating fast fracture zone and striations showing the crack propagation directions were found at different crack propagation regions (Fig. 18).

In most of the samples, smooth and burnished region was observed as a result of rubbing and an example of it is shown in Fig. 19a. When the sample (HAZ; $\sigma = 380$ MPa)

was examined with SEM in Fig. 19, tear ridge like patterns coalescing toward the crack propagation direction were observed at the center of the specimen and dimples
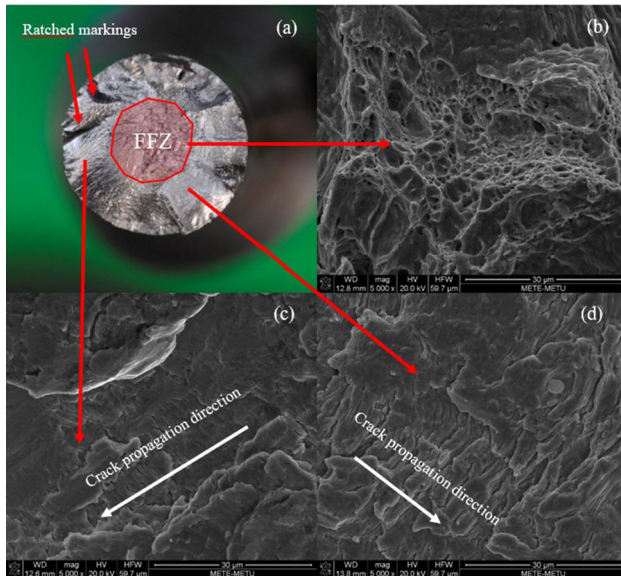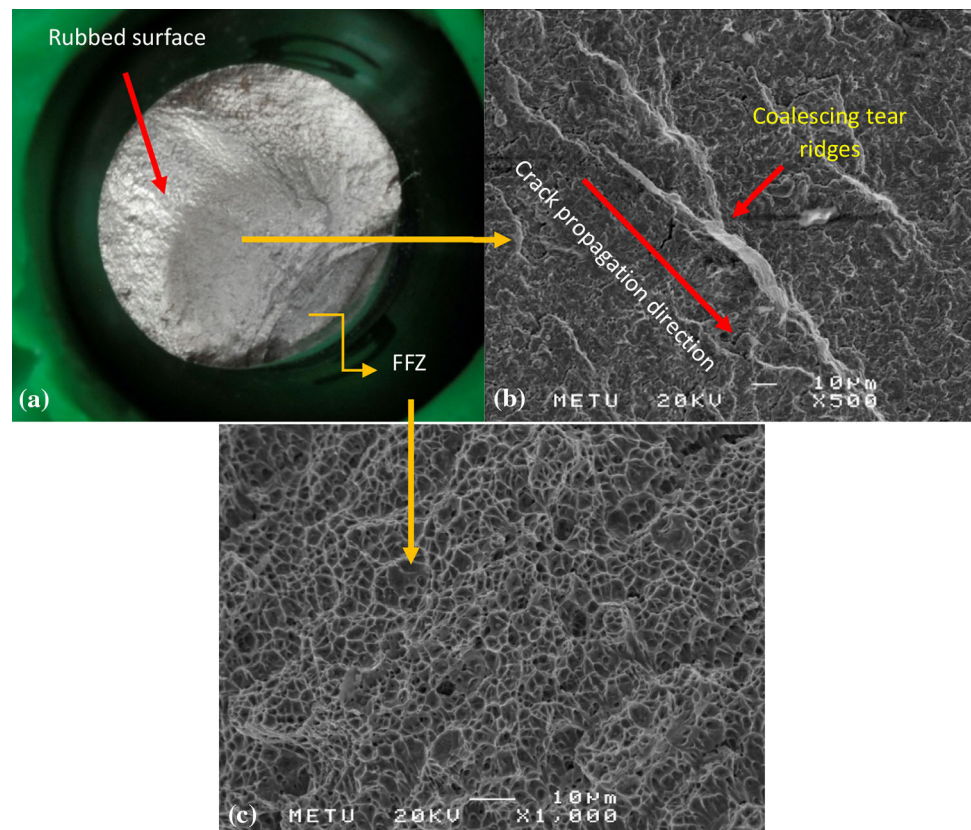

Fig. 18 Fracture surface of base metal ($\sigma = 434$ MPa); (**a**) ratchet markings and FFZ (fast fracture zone), (**b**) dimples indicating rapid failure and (**c**) and (**d**) striations indicating crack propagation direction

indicating transgranular ductile fracture at FFZ (fast fracture zone) are shown.

Figure 20 shows the welded specimen's fracture surface (failed at $\sigma = 379$ MPa). Due to rubbing of bottom and top of the crack, the crack initiation site and a part of the crack propagation region seemed dark in SEM analysis and no findings were found. Dimples were observed in rapid failure region and tear ridge like patterns in the direction of crack propagation were shown.

Striation Counting

Using striation counting method as shown in Figs. 21, 22 and 23, striation width was measured at a certain point and the distance between that point and the crack initiation point was measured. Striation width was measured more than one at the same region and the measured values were averaged to reach the nearest correct result. Stress intensity factor (ΔK) was calculated by using the formulas for a surface crack in a solid cylinder stated in "Mechanical Analysis" section. Bu using measured distances and calculations, crack propagation rate (da/dN) versus stress intensity factor (ΔK) was plotted in log scale for all test groups (Fig. 24). The curves represent the region where Paris power law is valid [19]. Coefficient of determination (R^2) values are 0.97 and 0.94 for HAZ and base metal,

Fig. 19 Fracture surface of HAZ ($\sigma = 380$ MPa); (**a**) rubbed surface and FFZ (fast fracture zone), (**b**) tear ridge like patterns coalescing toward crack propagation direction, (**c**) dimples indicating rapid failure

Fig. 20 (**a**) Fracture surface of welded specimen (failed at σ = 379 MPa), (**b**) dimples indicating rapid failure region, (**c**) rubbed surface and (**d**) tear ridge like patterns showing the direction of crack propagation
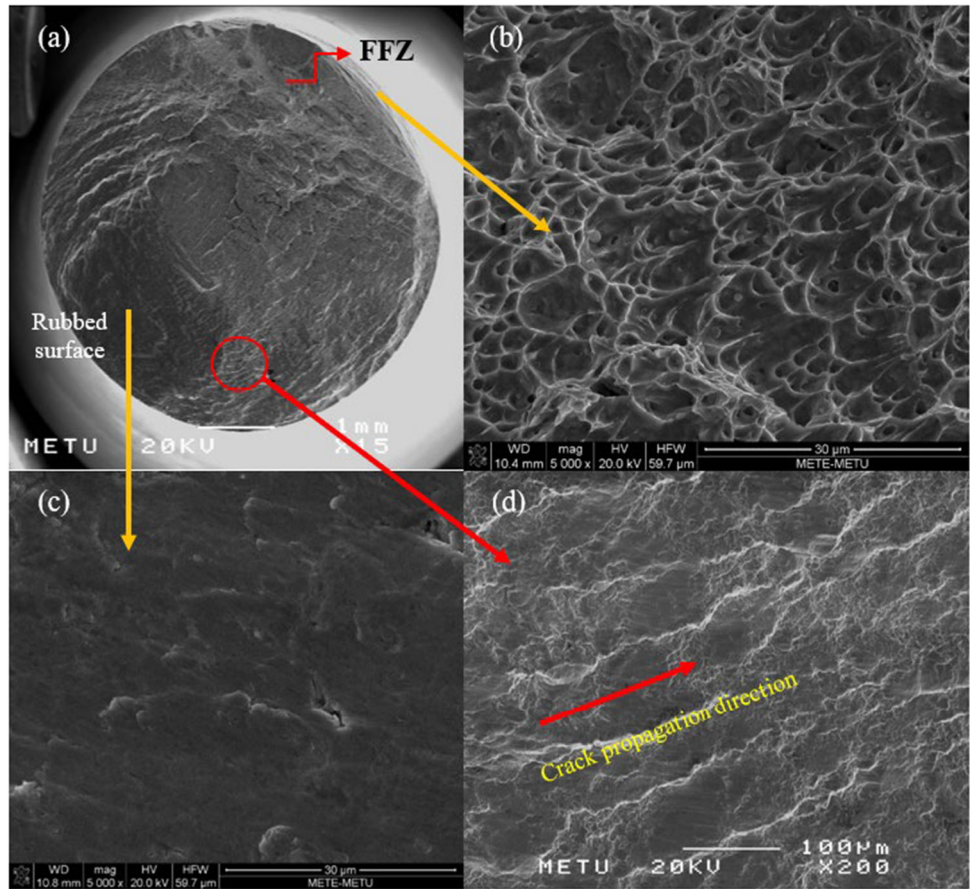

Fig. 21 SEM images of base metal fracture surface; (**a**) striation measurement point, (**b**) striation width measurements
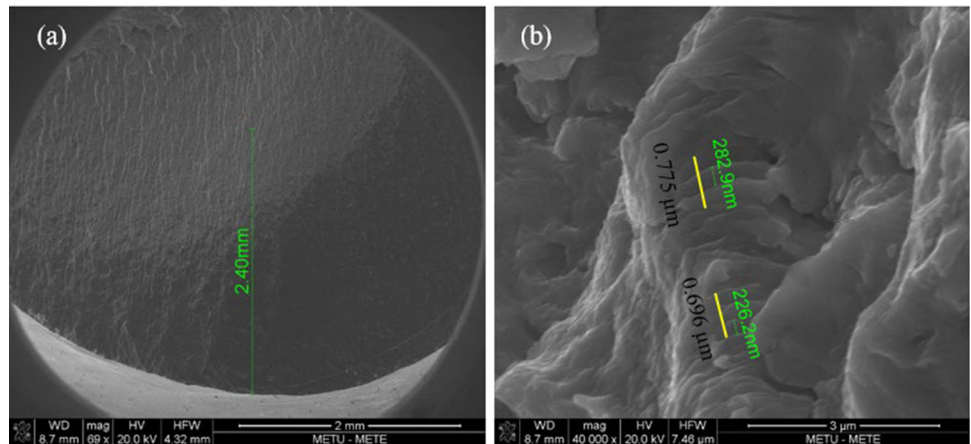
Fig. 22 SEM images of welded metal fracture surface; (**a**) crack initiation point, (**b**) striation width measurement at 3.32 mm away from crack initiation point
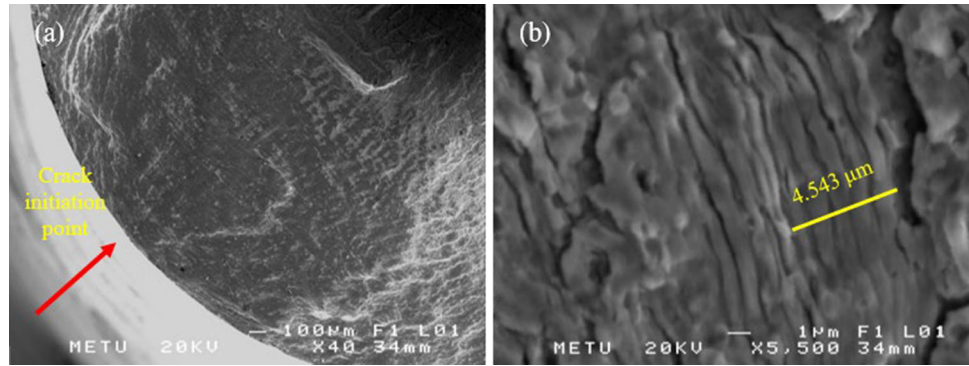

Fig. 23 SEM images of HAZ fracture surface; (**a**) crack initiation point, (**b**) striation width measurement at 3.34 mm away from crack initiation point
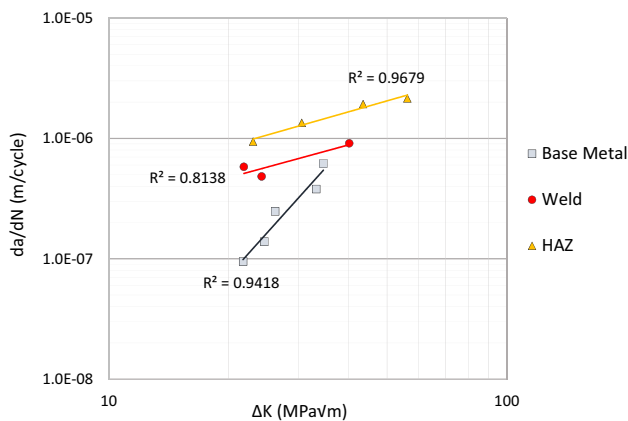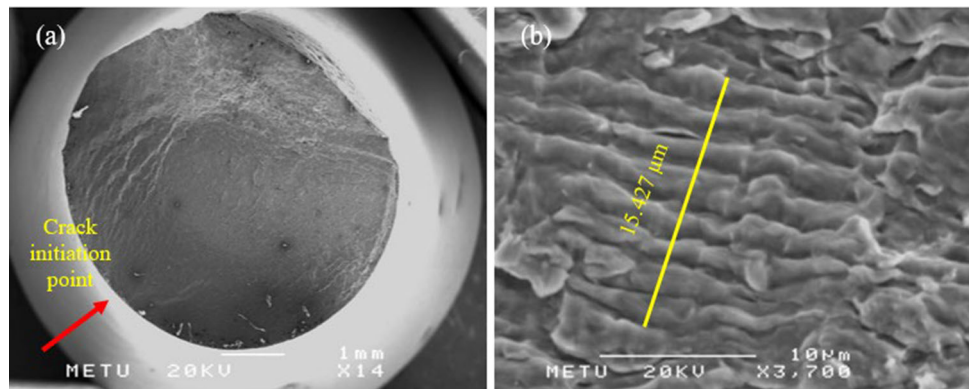

Fig. 24 Crack growth behavior of base metal, weld and HAZ

respectively, indicating the reliability of curve fitting. However, it is 0.81 for weld due to lack of striation spacing measurement data. As can be seen from Fig. 24, crack growth rate is lowest for base metal at same ΔK value up to approximately 40 MPa$\sqrt{}$m, showing that base metal has better performance than weld and HAZ. The Paris slope (m) for base metal is 3.68 which is a reasonable value for a HSLA steel.

Conclusion

The fatigue behavior of base metal, weld and HAZ regions of welded API X70 pipeline steel was compared from point of crack initiation and propagation. As a result of this study, the following results were achieved.

- Tensile properties of base metal and weld were found to be almost the same. Charpy impact test results show that base material has approximately twice impact energy than weld and HAZ at room temperature. However, Charpy impact energies of HAZ and weld decreased noticeably at − 30 °C, while very slight decrease was observed for base metal. The reason for base metal having better toughness than weld and HAZ can be explained by fine and acicular ferrite obtained as a result of TMCP. Very close values were obtained due to hardness measurements of base metal, weld and HAZ.
- The fatigue life of weld at any stress level is lower than base metal and HAZ, and this makes weld a potential region for possible crack initiation. This could be the result of surface irregularities and possible defects in weld region that increase the crack susceptibility of weld. At stress values applied below 380 MPa, base metal has better performance than HAZ. The fatigue

ratios of all three test groups were found to be within the range specified for steels.

- Crack growth rate was found to be lowest for base metal at same ΔK values up to approximately 40 MPa$\sqrt{m}$. This result is also compatible with Charpy impact test results; the base metal having the highest toughness has higher resistance to crack propagation.

- The Paris slope (m) for base metal was found as 3.68 which is a reasonable value for a HSLA steel. This result shows that striation counting can be used as a fractographic approach in order to estimate the crack growth behavior of materials.

References

1. M. Bilen, *Uygulanan Testler ve Mekanik Özelliklerinin İyileştirilmesi* (2016), pp. 960–963
2. L.B. Godefroid, L.C. Cândido, R.V.B. Toffolo, L.H.S. Barbosa, Microstructure and mechanical properties of two Api steels for iron ore pipelines. Mater. Res. **17**, 114–120 (2014)
3. N. Engin, Z. Erman, "Düzce Üniversitesi Bilim ve Teknoloji Dergisi," *Düzce Üniversitesi Bilim ve Teknol. Derg.*, vol. 4, no. Doğadan Esinlenen Optimizasyon Algoritmaları ve Optimizasyon Algoritmalarının Optimizasyonu (2016), pp. 293–304
4. S.Y. Shin, B. Hwang, S. Kim, S. Lee, Fracture toughness analysis in transition temperature region of API X70 pipeline steels. Mater. Sci. Eng. A **429**(1–2), 196–204 (2006)
5. L. Gajdoš, M. Šperl, J. Bystrianský, Fatigue behaviour of X70 steel in crude oil. Mater. Tehnol. **49**(2), 243–246 (2015)
6. J. Capelle, J. Gilgert, G. Pluvinage, Hydrogen effect on fatigue and fracture of pipe steels
7. G. Üniversitesi Fen Bilimleri Dergisi, S. Aksöz, H. Ada, A. Özer, Toz Altı Ark Kaynak Yöntemiyle Üretilen API 5L X70 Kalite Çelik Boruların Mikroyapı ve Mekanik Özellikleri, vol. 5, no. 1, pp. 55–64 (2017)
8. K. Miková, S. Bagherifard, O. Bokuvka, M. Guagliano, L. Trško, Fatigue behavior of X70 microalloyed steel after severe shot peening. Int. J. Fatigue **55**, 33–42 (2013)
9. L. Ligang et al., Evaluation of the fracture toughness of X70 pipeline steel with ferrite-bainite microstructure. Mater. Sci. Eng. A **688**(January), 388–395 (2017)
10. J. V. S. J. S. P. J. K. J Billingham, Review of the performance of high strength steels used offshore (2003)
11. Z. Tas, Examination of mechanical properties and weld zone of X70 pipe steel after welding. Int. J. Sci. Technol. Res. **06**(07), 148–152 (2017)
12. S. Apay, M. Gel, G. Çil, Tozaltı Kaynak Yöntemi ile Farklı Kaynak Parametreleri Kullanılarak Birleştirilen API X70M PSL2 Malzemelerin Kaynak Bölgesinin İncelenmesi. Düzce Üniversitesi Bilim ve Teknol. Derg. 6(4), 714–723 (2018)
13. A.A. Akay, Y. Kaya, N. Kahraman, Tozaltı Ark Kaynak Yöntemi ile Birleştirilen X60, X65 ve X70 Çeliklerin Kaynak Bölgesinin Etüdü. Karaelmas Sci. Eng. J. 3(2), 34–42 (2013)
14. P. Simion, V. Dia, B. Istrate, G. Hrituleac, I. Hrituleac, C. Munteanu, Study of fatigue behavior of longitudinal welded pipes, *IOP Conf. Ser. Mater. Sci. Eng.*, vol. 145, no. 2 (2016)
15. E. Drexler, R. Amaro, Fatigue crack growth rates of API X70 pipeline steels in pressurized hydrogen gas compared with an X52 pipeline in hydrogen service, *Int. Hydrog. Conf. (IHC 2016) Mater. Perform. Hydrog. Environ.* (2017), pp. 210–218
16. P.C. Miedlar, A.P. Berens, A. Gunderson, J.P. Gallagher, DTD Handbook | summary of stress intensity factor information | selected stress intensity factor cases, in *Damage Tolerant Design Handbook* (2002)
17. K. Lieb, R. Horstman, B. Power, R. Meltzer, M. Vieth, O. Vosikovsky, Effects of stress ratio on fatigue crack growth rates in X70 pipeline steel in air and saltwater. J. Test. Eval. **8**(2), 68 (1980)
18. W.D. Callister, D.G. Rethwisch, Materials Science and Engineering 9th Edition, *Comput. Sci. Eng.* (2014)
19. E. Poursaeidi, M. Sanaieei, H. Bakhtyari, Life estimate of a compressor blade through fractography. Int. J. Eng. Trans. A Basics **26**(4), 393–400 (2013)